Soft Matter

View Online
Dynamic Article Links

Cite this: DOI: 10.1039/c1sm06024d

www.rsc.org/softmatter

PAPER

Propagation of a brittle fracture in a viscoelastic fluid

Hervé Tabuteau,†[ab] Serge Mora,[ab] Matteo Ciccotti,[abc] Chung-Yuen Hui[d] and Christian Ligoure*[ab]

Received 1st June 2011, Accepted 21st July 2011
DOI: 10.1039/c1sm06024d

During pendant drop experiments, a model physical gel made from oil in water microemulsion droplets reversibly linked together by triblock copolymers, exhibit a very peculiar filament rupture corresponding to highly brittle failure of a viscoelastic fluid. The fracture propagation has been tracked by high speed videomicroscopy. Analysis of the time evolution of the fracture profile shows that the fracture is purely elastic and reversible without any significant bulk and interfacial viscous dissipation. However, since the elastic moduli of such complex fluids are low, hyper elastic corrections have to be taken into account for a quantitative analysis of the fracture profile. This brittle behavior is well explained by a hyperelastic generalization of the viscoelastic trumpet model of de Gennes. The velocity of the fracture's propagation is measured and compared to the predictions of a simple microscopic model.

1 Introduction

Although fracture mechanics were originally based on an equilibrium transformation between the mechanical energy stored in an elastic body and the surface energy that is necessary to produce a fracture in the body,[1] in most practical cases the high concentration of stress in the crack tip region implies the activation of dissipative processes that adsorb a large amount of energy, which is generally dominant in the energy balance of fracture propagation. This energy dissipation implies an irreversibility of fracture and a velocity dependence of the fracture energy $G(V)$.[2,3] In his famous seminal work Griffith[1] tested its energy balance criterion on a very brittle solid such as glass where energy dissipation is considered to be minimal. In less brittle materials such as polymers or metals, the fracture energy can be hundreds to thousands of times larger than the surface tension due to the high amount of plastic deformation in the neighborhood of crack tips.

Fracture in reversible physical gels is less documented and understood than in solid materials but attracts a great deal of interest in recent years.[4–16] Filament stretching extensional rheometry[8–10] or capillary breakup rheometry experiments[9,10] have been used to study the fracture of networks of associative polymers or solutions of entangled wormlike micelles, but these experiments were essentially limited to the measurements of extensional viscosities. On the other hand, quantitative analysis of the crack propagation and morphology in viscoelastic *solids* in planar geometry have been performed.[4,5,17] However, to the best of our knowledge, the systematic analysis of morphology and propagation of a crack in a viscoelastic *fluid* does not have been yet reported.

Here we present a system where the Griffith theory is applicable with an excellent approximation, consisting in a soft transient network gel in which nanodroplets of an oil-in water microemulsion are reversibly linked by telechelic polymers[18] (Fig. 1). This system is a model Maxwell fluid. Indeed, its linear rheological properties can be characterized by a shear plateau modulus μ_∞ and a single dominant relaxation time τ.[18] Moreover, it does not exhibit any shear thinning, nor shear thickening nor shear banding until it breaks, as shown from flow curves.[11,12,14] This is in contrast to the behaviour of one of the more popular Maxwell fluids, *i.e.* solutions of entangled wormlike micelles.

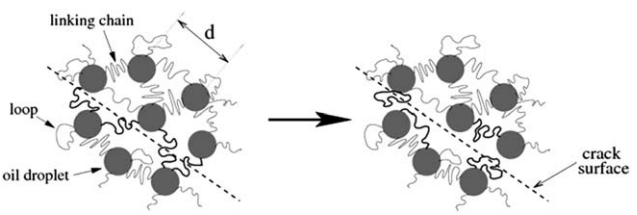

Fig. 1 A schematic of a bridged microemulsion. The telechelic polymers can either link two oil droplets or loop on a single one. (Left) Before the crack nucleation (bold dashed line) polymers can bridge oil droplets on both sides of the bold dashed line. (Right) When the crack occurs, the same polymers cannot cross the bold dashed line any more and form bridges in the other directions or loops.

[a]*Université Montpellier 2, Laboratoire Charles Coulomb UMR 5221, F-34095, Montpellier, France. E-mail: christian.ligoure@univ-montp2.fr*
[b]*CNRS, Laboratoire Charles Coulomb UMR 5221, F-34095, Montpellier, France*
[c]*Laboratoire PPMD-SIMM, UMR CNRS 7615, ESPCI, 10 rue Vauquelin, 75005 Paris, France*
[d]*Department of Theoretical and Applied Mechanics, 322 Thurston Hall, Cornell University, Ithaca, NY 14853, USA*
† Present address: Institut de Physique de Rennes, UMR UR1-CNRS 6251, Université de Rennes I, Bât. 11A, 35042 Rennes Cedex, France.

In a previous paper,[12] some of us have investigated the fracture initiation of this Maxwell fluid using a pendant drop experiment, which corresponds to a pure elongational stress condition due to the lack of contact with solid interfaces near the fracture region. We have shown that the fracture initiation process is governed by the thermally activated nucleation of a critical crack in the polymeric network. In this approach, the rupture stress was predicted to be on the order of the shear modulus, in very good agreement with experimental data. One of the key points to understand this mechanism of fracture is the bond reversibility and the corresponding relevant ultra low interfacial energy needed to nucleate the crack. This interfacial tension results from the loss of conformational entropy of polymeric bonds near a crack interface and is typically on the order of few μN m^{-1}.[19]

The aim of this paper is the rationalization and the quantification of the crack propagation for such a Maxwell fluid in this failure geometry, by a time-resolved analysis of the shape of the growing crack. We want to address the following questions: What is the fracture energy? What is the crack propagation speed? We will show that the fracture profile has a parabolic shape that can be rationalized using a finite elasticity theory[20,21] that needs to be used, because of the large deformations exhibited in this soft material. The only ingredients affecting the energy balance in the fracture mechanism of a brittle material are the bulk elastic modulus μ_∞ and the surface tension γ. According to such a description, the fracture energy G is substantially independent of fracture velocity (once the velocity is enough for having a purely elastic material response), and the crack velocity should only be limited to the Rayleigh waves propagation velocity.[22] However, for the complex fluid we consider, the propagation of the crack takes place at a constant velocity of the order of few mm s^{-1}, which is much smaller than the Rayleigh waves velocity in the gel $c_R \simeq 1$ m s^{-1}.

The origin for this characteristic velocity must be sought at the scale of the microscopic mechanisms of crack propagation, *i.e.* the debonding mechanisms of the polymer chains grafted on the oil droplets. The energetics of polymer debonding are very weak compared to the surface tension of the gel. This is constituted by a reversible term γ_{pol} associated to the free energy of purely entropic origin required to ungraft the polymers along a unit interface and an irreversible term associated to the Stokes dissipation caused by the motion of the oil droplet in the viscous fluid (water) that is necessary to propagate the stresses to the new crack tip. These two terms describe the wet fracture of the polymer network inside the solvent and our claim is that they determine the time scale for fracture propagation. However, they are both energetically very small in relation to the energy to create the two new interfaces between the gel and the air, and they are thus not easily accessible by experimentally measuring the fracture energy. The high degree of reversibility of the fracture is thus related to a significant decoupling between the mechanisms of creation of new gel/air interfaces (which dominate the energetics) and the mechanisms of network bond breaking on the polymer scale (which determine the time scales for crack propagation).

The paper is organized as follow. Section 2 is devoted to materials and methods. The time resolved analysis of the fracture profiles is reported in section 3. Section 4 presents a review of the viscoelastic trumpet model of de Gennes for a Maxwell fluid and its tentative extension to the hyperelastic case. In section 5, a simple theoretical approach is proposed to understand the velocity of fracture propagation. Finally, in section 6, the experimental results are discussed in the framework of the models developed in sections 4 and 5.

2 Materials and methods

2.1 Description of the transient network gel

The system we used is composed of an oil-in-water droplet microemulsion to which telechelic polymers are added (Fig. 1). This system was previously described by Filali *et al.*[23] The o/w microemulsion involves a cationic surfactant, cetyl-pyridinium chloride CPCl, and a cosurfactant *n*-octanol. The droplets are swollen with decane and dispersed in 0.2 M NaCl brine. The droplets are spheres of radius $b = 62$ Å and were found to be robust to variations of both the microemulsion concentration and of the amount of added polymer.[23] The volume fraction in oil droplets is fixed to $\phi = 10\%$. The polymer chains (Poly-ethylene oxide) of molecular weight 10 kDa are grafted at both ends with aliphatic chains of eighteen CH_2 groups. After modification, the degrees of substitution of the hydroxyl groups were determined by NMR and were found to be larger than 98%. These hydrophobic end groups (stickers) anchor reversibly into the microemulsion droplets. The polymer amount is represented by the apparent connectivity R, *i.e.* the average number of hydrophobic stickers per droplet. Far above the percolation threshold this model system behaves as an elastic network with a shear modulus $\mu_\infty = nk_BT$ (n is the number density of linking chains, k_B the Boltzman's constant, T the temperature).[18] In this regime the connectivity is higher than 5. In this study we use two fluids with the connectivity equal to 6 and 12. In the following, we named those fluids R6 and R12.

2.2 Rheological properties

The linear properties of all the samples are Maxwellian[18] (Fig. 2). The elastic shear modulus μ_∞ is controlled by the density of the

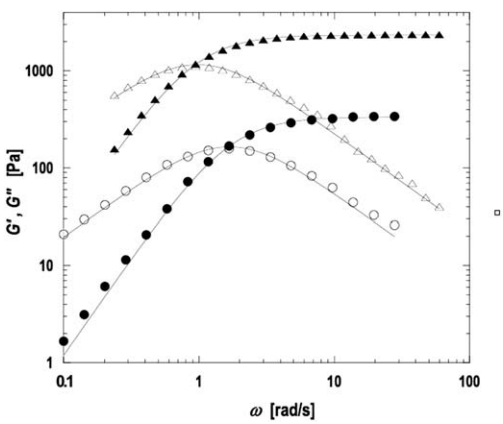

Fig. 2 Frequency sweep experiments (strain amplitude: 10%). Storage modulus, G', (filled symbols) and loss modulus, G', (unfilled symbols) as a function of the frequency ω for the fluids R6 (circles) and R12 (triangles). Solid lines correspond to fits by a Maxwell model which give us the elastic shear modulus and the relaxation time of each fluid.

active polymer and the terminal time τ is determined by the average residence time of the hydrophobic stickers in the oil droplets. Since the material is incompressible, which implies that its Poisson ratio is $\nu = 0.5$, the Young modulus is $E_\infty = 3\mu_\infty$. All the rheological measurements were performed with an RFS III controlled-strain rheometer at 23 °C. The shear modulus and the relaxation time are, respectively, equal to 330 Pa and 0.6 s for R6, and 2400 Pa and 2 s for R12.

2.3 Fracture experiments

We carried out pendant drop experiments with our fluid. This very simple test allows us to get a pure elongational flow, without the influence of a solid surface on the flow properties as is the case in the gap of an extensional rheometer. A syringe pump (KDS 200 from KD Scientific, USA) was used to form the drops with a fixed volume of 50 µl at a constant rate of 2 ml h^{-1} for both fluids. The material, initially in the syringe, flows through a lower plastic tube of a diameter of 2.596 mm and a drop emerges at the tube outlet that is enclosed in a glass box to reduce air currents. These conditions ensure that no elastic instability modifies the extensional flow while the drop starts to form underneath the tube. All the experiments were performed at room temperature of 23 °C. We use regular image analysis to determine the length and the radius of the drop. We also use a fast camera (Photron FastCam PCI CCD camera) equipped with a macro lens to study the fracture propagation with a pixel size resolution of 8×8 µm^2. The images were analyzed using NIH ImageJ (NIH, freely available for download at the ImageJ website URL: http://rsb.info.nih.gov/ij/). The fracture movies have been selected in such a way that the fracture propagates in a plane perpendicular to the camera direction. However, in most of the experiments the crack may nucleate everywhere around the filament and then the fracture propagates in a plane which is not orthogonal to the camera direction. Approximately 50 experiments were performed for each fluid in order to meet the orthogonality condition in a couple of cases where the fracture profile was then analyzed. We got the critical stress at the rupture of the drop σ_f in the following way. We measured the diameter D_0 of the drop where the fracture occurs and we weighted the mass of the falling part with the help of a laboratory balance of accuracy 1 mg (TP 303 Denver Instrument, Germany) placed underneath the injection set-up. In this condition the stress is measured with a precision of 5%. Finally the stress at the rupture is equal to $\sigma_f = mg/(\pi R^2_{\text{rupture}}) - 2\gamma_s/D_0$ with γ_s/D_0 the radial stress corresponding to the Laplace pressure and $mg/(\pi R^2_{\text{rupture}})$ is the tensile stress corresponding to the weight of the failing part of the drop at the rupture.

3 Results

The sequence of images in Fig. 3 shows the evolution of the drop under gravity from its formation to the final break-up for the R6 fluid. After the injection of the fluid there is the formation of a drop followed by the stretching of the filament by the falling drop. The flow can be separated in two regimes. In the first regime, the drop of fluid begins to fall when its weight exceeds the surface tension retaining force. This balance of forces determines the length scale of the drop, which is about 2 mm. The resulting

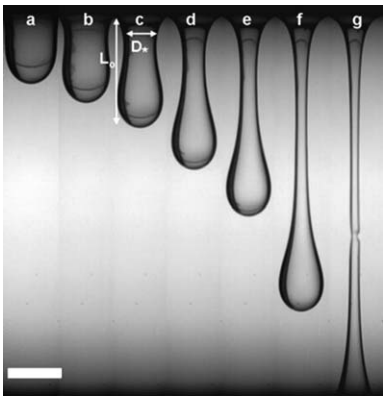

Fig. 3 A sequence of images of the fall of the R6 fluid. Regime 1 corresponds to images a and b and regime 2 corresponds to images c to g. At the beginning of regime 2 we define the radius of the filament $R_* = D_*/2$ and L_0, the length of the drop. The white scale bar corresponds to 2.5 mm.

flow results from the balance between the surface tension, the viscous force and the weight (Fig. 3a and b). In a second regime (Fig. 3 images c to g), the filament is stretched by the falling drop, whose shape remains approximately constant and is parabolic. In this regime, the drop has an initial length L_0 and the initial radius of the filament is R_* (Fig. 3c).

In the following, we suppose that inertia is negligible because we work with very viscous fluids (Reynolds number is of the order of 0.01). The filament is assumed to be a cylinder in an extensional flow, assuming that there is no flow from the filament into the drop. The evolution of the radius R, normalized by R_*, with time in regime 2 and the corresponding sequence of images of the fall are very similar to those predicted by the inertialess slender-drop theory and finite element computation of Stokes *et al.*[24] (*cf.* Fig. 4). The filament thinning is rather slow and its dynamics can be described by a simple balance between the viscous and gravitational forces, the surface tension being neglected. The variation of the radius filament is given by

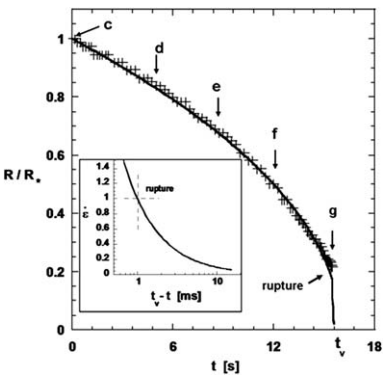

Fig. 4 The minimum radius R along the filament *versus* time for the R6 fluid (crosses). The letters on the graph corresponds to the labels on the images of Fig. 3. The black line corresponds to the fit of the data by the formula defined by Stokes for the purely viscous fall,[24] with $L_0 = 5.25$, $t_v = 15.57$ s and $R_* = 0.84$ mm. The variation of the deformation rate against the time left to break-up ($t_v - t$) deduced from this formula is plotted in the inset. The dashed cross corresponds to the moment where the fracture occurs.

$R(t) = R_*(1 - t/2t_v)^{1/2}$ with $t_v = 3\eta/(\rho g L_0)$. L_0 is the initial length of the drop in the second regime, ρ is the mass density and g gravity's acceleration (*cf.* Fig. 4). Most of the thinning process of the filament takes place during this viscous fall for R_* down to $0.2R_*$. For smaller radii there is a fast rupture of the filament (Fig. 3g), described in detail later on, corresponding to the fracture propagation. From the above expression of the time evolution of the radius we calculate the deformation rate, $\dot{\varepsilon} = -2/R(\mathrm{d}R/\mathrm{d}t)$(see inset of Fig. 4). In this way, we get the deformation rate when the fracture starts to propagate, which is equal to 1 s^{-1} and 0.06 s^{-1} for R6 and R12 fluids, respectively. It is interesting to notice that elastic effects do not affect the time variation of the radius of the filament for $t > \tau$[25] and so are not visible in Fig.4 because $\tau = 0.6$ s. The total duration of the fall before the opening of a crack is typically on the order of 50 to 200 s, much larger than the relaxation time of the Maxwell fluid $\tau \lesssim 1$ s. The tensile stress increases because of the decrease of $R(t)$, until a crack nucleates at the surface of the filament for a critical stress $\sigma_f \simeq 0.5E$.[12] Then the fracture propagates across the sample and eventually leads to the rupture of the drop (Fig. 5a). In the experiments presented here, the fracture mechanism is a two step process. It has been shown in a previous paper,[12] that the first step consists of a spontaneous nucleation

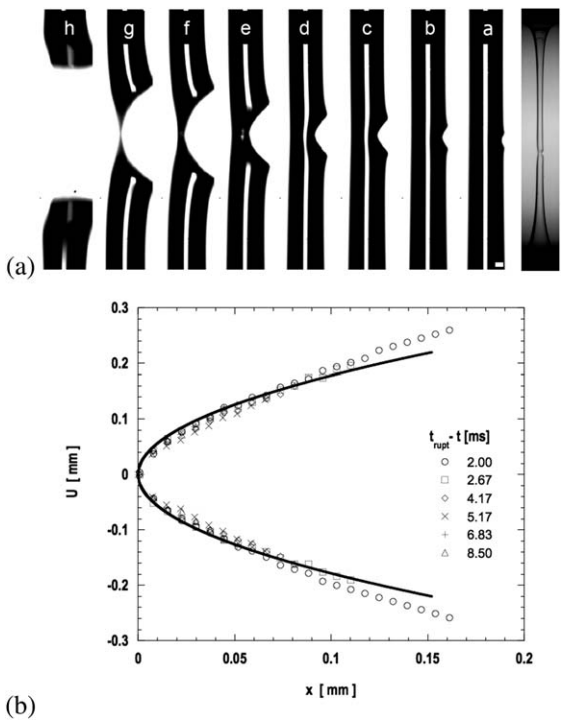

Fig. 5 (a) Pictures of the propagation of the fracture across sample R6 from the right to the left. The time left to achieve complete fracture of the filament corresponding to each picture labelled with a letter is: a (8.50 ms), b (5.16 ms), c (2.67 ms), d (2.00 ms), e (1.00 ms), f (0.33 ms), g (0.17 ms) and h (0.ms). The last picture on the right shows almost all of the elongated drop, with the crack being well developed. The white scale bar corresponds to 0.1 mm. (b) Fracture profiles $u(x)$ for different times before the break-up in the fracture moving frame, corresponding to the pictures of the part a of this figure. The black line is a parabolic fit corresponding to eqns (1) and (2) with $J = 2\gamma_s$. We report only the profile for $L < 0.1D_0$.

(thermally activated crack) of a microcrack within the oil droplet/telechelic polymers network, the microcrack being filled up with solvent. In the following we discuss in detail the second step, which corresponds to the destabilization of the capillary bridge and the propagation of a dry fracture through the material.

It is worth noting that from the beginning of the propagation up to the complete fracture (*i.e.*, when the sample is separated in two parts) the fracture profile exhibits a parabolic shape (Fig. 5a) as expected for an elastic solid breaking under tension. These observations were confirmed by quantitative analysis of the fracture profile $u(x)$ on the overall crack propagation across the sample. Different fracture profiles measured in the fracture moving frame and a parabolic fit

$$u(x) = a\sqrt{x} \tag{1}$$

are represented in Fig. 5b.

We could be tempted to interpret this parabolic shape according to the linear elastic fracture mechanics solutions:[26]

$$u(x) = \frac{K_I}{E'}\sqrt{\frac{8x}{\pi}}$$

where the (local) stress intensity factor K_I can be bound to the strain energy release rate by $G = K_I^2/E(1 - \nu^2)$, but in soft solids the crack tip region exhibits very large deformations that require the use of finite elasticity theories.[27] The finite elasticity formalism for crack tip stress and displacement fields in a Neo-Hookean solid is developed in the Appendix 1 for a 2D plane strain problem. The nonlinear character of the problem requires the fracture energy to be estimated by the J-integral method[28] (the method is summarized in Appendix 1) and it can be related to the parameter a of the parabolic crack opening profile by:

$$J = \frac{\pi\mu_\infty a^2}{4} \tag{2}$$

One of the main aims of the present work will be to show that finite elasticity fully describes the behavior of our gel during this rapid fracture experiment (*cf.* sections 4 and 6). This local estimation of the J-integral thus also provides an estimate of the strain energy release rate $G = J$.

We stress the point that the use of eqn (2) essentially assumes a 2D symmetry of the crack profile, which is not realistic in the case of a cylindrical filament. However, since the movie has been selected in order to present an excellent orthogonality between the camera orientation and the direction of crack propagation, the observed opening profile provides a good local estimate of the fracture energy, the measurement being more accurate for shorter cracks.

The variation of the estimated fracture energy G and the measured length of fracture L as a function of the time to rupture $t_{rupt} - t$ are represented in Fig. 6. Two distinct regimes are clearly evident depending on the length of the crack:

(i) for $L < 0.1D_0$, both the fracture energy and the crack speed remain almost constant with values roughly equal to $G \approx 90$ mJ m^{-2} and $V = 4$ mm s^{-1}. It turns out that the estimated value for G is roughly twice the surface tension $\gamma_s \simeq 45$ mJ m^{-2} of the solvent, *i.e.* the stabilised oil-in-water droplet microemulsion without telechelic polymers. We remark firstly that the surface energy needed to pull-out the hydrophobic stickers from the oil

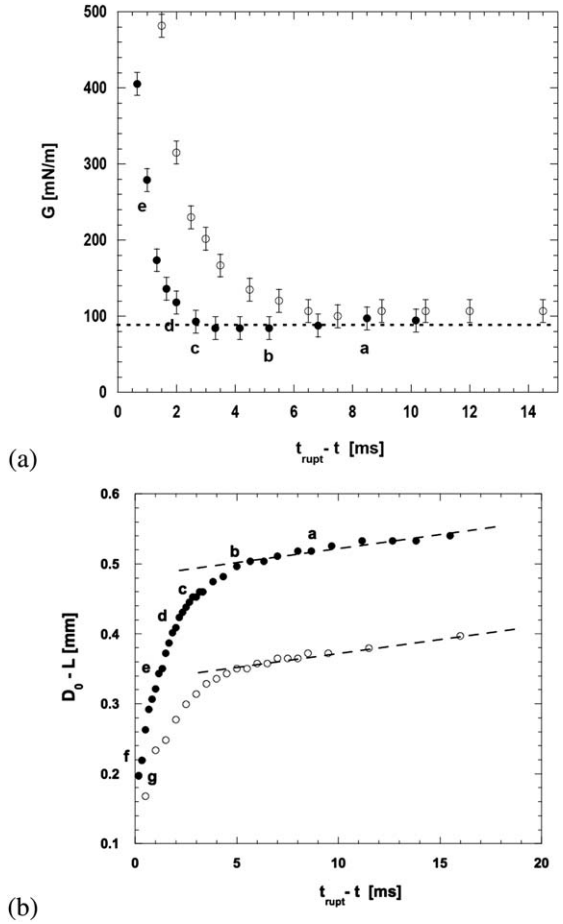

Fig. 6 (a) Fracture energy *versus* the time before complete fracture $t_{rupt} - t$ for R6 (filled circles) and R12 (unfilled circles) fluids. The letters still correspond to the picture in Fig. 5a associated with the R6 fluid fracture. The dotted line corresponds to $G = 2\gamma_s$. (b) Evolution of the total length of the fracture L ($D_0 - L$ in the graph) with the time before complete fracture $t_{rupt} - t$. The legend is the same as for part a. The diameter of the filament when the crack occurs at the surface of the material D_0 is equal to 0.584 and 0.407 mm for R6 and R12 fluids, respectively. The dotted lines correspond to the linear fit of the data which gives a constant crack speed $V = dL/dt = (4.00 \pm 0.02)$ mm s^{-1}.

droplet γ_{pol}, of the order of 10 μN m^{-1} [12] is completely negligible. Secondly, the relation $G \approx 2\gamma_s$ strongly supports the proposal that there is no significant dissipative contribution in the crack tip region. In this regime the crack speed is also constant and is roughly equal to 4 mm s^{-1} (Fig. 6b)

(ii) for $L > 0.1D_0$, the estimated fracture energy and the crack speed increase when we go closer to the complete break-up of the filament. It's worth noting that the results concerning G must be interpreted with caution as the finite size effect may be important. It is then questionable whether the use of eqn (2), valid for a 2D plane strain geometry, is still justified.

4 Hyperelastic correction of the trumpet model for the fracture in a Maxwell fluid

In order to provide a rationale for the presented behaviour, we propose here a development of the de Gennes model of the viscoelastic trumpet,[17,29,30] which presents a qualitative theoretical analysis of the dissipative processes during the bulk fracture in a viscoelastic material. This model was initially conceived to explain at the level of scaling laws the remarkable relation between the fracture energy per unit area $G(V)$ at crack velocity V and G_0, the limiting value of the fracture energy at zero crack rate that was reported for elastomeric materials:[2,3]

$$G(V) = G_0 + G_V(V) = G_0(1 + \phi(a_T V)) \quad (3)$$

where a_T is the temperature shift factor given by the Williams-Landel-Ferry equation.[31]

A similar argument can be used to express the fracture energy for a fracture of length $L(t)$ moving at velocity V. The trumpet model predicts the following scaling form for the dissipated energy term $G_V(V)$:

$$G_V(V) \simeq \frac{T\dot{S}}{V} \simeq \frac{1}{V}\int \mathrm{d}x\mathrm{d}y\sigma\dot{\gamma} = \frac{1}{V}\int \mathrm{d}x\mathrm{d}y Re\left[\frac{\underline{\sigma}\,\underline{\dot{\gamma}}^*}{2}\right]$$
$$= \frac{1}{V}\int r\mathrm{d}r \frac{\sigma_0^2}{2}\frac{\omega\mu''(\omega)}{\mu'(\omega)^2+\mu''(\omega)^2}\Bigg|_{\omega=V/r} \quad (4)$$

where the complex strain $\underline{\gamma}$ is related to the complex stress $\underline{\sigma}$ through $\underline{\gamma} = \underline{\sigma}/\mu(\omega)$ and the distance to the crack tip r is related to the frequencies of the excitation ω by the scaling relation $\omega(r) = V/r$. T is the temperature, $\dot{S}$ is the entropy creation rate and $\sigma_0 = |\underline{\sigma}|$.

The complex modulus $\mu(\omega)$ of a Maxwell fluid as function of frequency is the following:

$$\mu(\omega) = \mu'(\omega) + i\mu''(\omega) = \mu_\infty \frac{i\omega\tau}{1+i\omega\tau} \quad (5)$$

At low frequency ($\omega\tau \ll 1$), the modulus is purely imaginary ($\mu = i\omega\mu_\infty\tau$) and the material behaves as a liquid of viscosity $\eta = \mu_\infty\tau$. At high frequency ($\omega\tau \gg 1$) we are dealing with an elastic solid of elastic modulus $\mu \approx \mu_\infty$. So from eqns (4) and (5), one gets

$$\frac{\mu''(\omega)}{\mu'(\omega)^2+\mu''(\omega)^2} = \frac{1}{\mu_\infty\omega\tau} \quad (6)$$

Putting eqn (6) into (4) one gets

$$G_V(V) = \frac{V}{2\mu_\infty\tau}\int_{\omega_{min}}^{\omega_{max}} \sigma_0^2 \frac{d\omega}{\omega^3} \quad (7)$$

where the limiting values $\omega_{min} = V/L$ and $\omega_{max} = V/\ell$ define the range of frequency over which the material is excited, ℓ being the length of a small microscopic nonlinear zone, typically on the order of 100 Å[17] (see Fig. 7).

4.1 Linear elastic case

de Gennes analysis is founded on the consideration that for a viscoelastic medium, the scaling law for the stress σ as a function of the distance r from the crack tip is still equivalent to that which we have for a steadily growing mode I interface in plane stress or plane strain in an elastic medium $\sigma \simeq K_I/\sqrt{r} \approx K_I\sqrt{\omega/V}$, where K_I is the applied stress intensity factor, and $G_0 = K_I^2/\mu_\infty$ is the fracture energy that would be

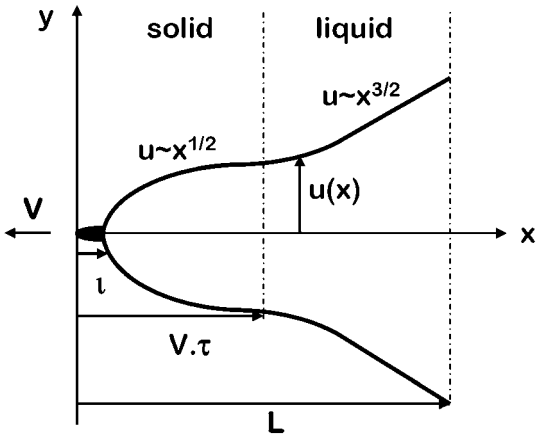

Fig. 7 A schematic representation of the space and time scales associated to a crack of length L moving with velocity V in a Maxwell fluid according to the trumpet model.[17] A small microscopic nonlinear zone of length ℓ is represented in black. The behaviour of the material is solid like at scales smaller than $V\tau$, then fluid like at larger scales.

present in an elastic medium under the same conditions. Eqn (7) for the dissipated energy thus reads:

$$G_V(V) = \frac{K_I^2}{\mu_\infty \tau}\left(\frac{1}{\omega_{\min}} - \frac{1}{\omega_{\max}}\right) = G_0\frac{L-\ell}{V\tau} \simeq G_0\frac{L}{V\tau} \qquad (8)$$

And so, if $L < V\tau$, then $(G(V) - G_0)/G_0 \simeq L/V\tau < 1$, and the bulk viscous dissipation is negligible. It is convenient to express this characteristic ratio as:

$$\frac{L}{V\tau} = \frac{t^*}{\tau} \qquad (9)$$

where $t^* = L/V$ is the characteristic time of propagation of a crack of length L at the velocity V. The condition for neglecting dissipation just reads $t^* < \tau$: the characteristic time needed to create a crack of length L is smaller than the relaxation time of the viscoelastic fluid.

For a simple Maxwell fluid exhibiting a crack propagation we can distinguish three spatial regions with different properties corresponding to three regimes of frequencies:

(i) $0 < x < \ell$: directly ahead of the crack tip there is a small microscopic nonlinear zone of length ℓ, independent of the separation rate, where the fracture process leads to the term G_0 of the fracture energy in eqn (3).

(ii) $\ell < x < V\tau$: in this region, the complex modulus is essentially real ($\mu(\omega) \approx \mu_\infty$), the viscous dissipation is negligible and the material can be considered as an elastic solid.

(iii) $V\tau < x < L(t)$: in this region, the complex modulus is essentially imaginary ($\mu(\omega) \approx i\omega\mu_\infty\tau$) and the material can be viewed as a Newtonian liquid of viscosity $\eta = \mu_\infty\tau$. Only this region contributes to the bulk viscoelastic dissipation processes.

From this model several interesting features appear:

(i) The characteristic value G_0 of the fracture energy is governed by the small nonlinear zone of size ℓ near the crack tip and equals the Dupré work $G_0 = 2\gamma_s$ needed to cut the material in air, γ_s being the surface tension of the fluid.

(ii) If the fracture length is small ($\ell < L(t) < V\tau$), according to eqn (8) viscous dissipation does not occur and $G(V) = G_0$. This regime takes place at short propagation times $t^* < \tau$ and can constitute the whole crack propagation if there is some maximal cut-off for the fracture length $L_{\max} < V\tau$, as is the case for the filament rupture experiment reported in this paper, where $L_{\max} = D_0 \approx 600$ μm is the diameter of the filament just before failure. In this purely elastic regime of the fracture propagation, where the viscous region does not appear because of the finite size of the sample, the profile $u(x)$ of the fracture should be parabolic,[28] and should not depend on the rate of propagation of the fracture.

(iii) Viscous dissipation will occur only if $L_{\max} > V\tau$. In this regime, eqn (8) shows that $G(V) > G_0$, provided that ℓ remains small with respect to the sample dimension. In this zone ($V\tau < x < L(t)$), de Gennes has shown that the scaling form $\sigma \sim x^{-1/2}$ for the stress components remains valid for a viscoelastic medium leading to the expected profile $u(x) \sim x^{3/2}$. The sign change in the concavity of the fracture profile at $x \sim V\tau$ is at the origin of the name "trumpet" for this model. Such a trumpet profile has been experimentally observed for adhesive fractures in polymer melts.[17]

4.2 Hyperelastic case

The crack tip stress singularity mathematically implies very large strains in a region close to the crack tip with a characteristic size $R_{\text{tip}} \sim G_0/\mu_\infty$ that questions the application of linear elasticity to fracture mechanics.[27] For most materials this region is smaller than the fracture process zone and is thus not relevant. However, for very soft materials this region can become significant and must be taken into account. Four our gels it should be in the 100 μm range, which is large compared to the small cohesive zone ℓ and it is of the same order of magnitude as the characteristic diameter of the breaking gel filament. We discuss in this section the generalization of the de Gennes argument to the estimation of the dissipated energy in the hyperelastic case.

The crack tip solutions for plane strain finite elasticity are discussed in Appendix 1, as well as the computation of the J integral. When considering the scaling of the true Cauchy stress $\sigma^{(C)}$ (eqn (34)), which is the most physically relevant description of stress, we remark that the stress components present different scaling relations as a function of the distance r from the crack tip, notably r^0, $r^{-1/2}$and r^{-1}. The second one is the same as in the linear elastic case. At the level of the scaling law analysis of the trumpet model, and omitting all numerical prefactors, we can estimate the contributions of each component of the Cauchy stress tensor to the dissipated energy from eqns (7) and (34).

The r^0 component $\sigma_{11}^{(C)}$ gives the contribution $G_V^{(11)}(V)$ to the viscous dissipated energy:

$$G_V^{(11)}(V) \sim \frac{V}{2\mu_\infty\tau}\int_{\omega_{\min}}^{\omega_{\max}}\left(\sigma_{11}^{(C)}\right)^2\frac{d\omega}{\omega^3} \simeq \frac{L^2\mu_\infty C^4}{V\tau} \qquad (10)$$

where, as discussed in Appendix 1, $C \approx 1$and the scaling of the J integral is $J \simeq \mu_\infty a^2$ (eqn (2)). We can thus rewrite eqn (10) as:

$$\frac{G_V^{(11)}(V)}{J} \sim \frac{L}{a^2}\frac{L}{V\tau} = \frac{L}{R_{\text{tip}}}\frac{t^*}{\tau} \qquad (11)$$

where $R_{\text{tip}} \sim J/\mu_\infty \simeq a^2$ is the radius of curvature of the crack tip and $t^* = L/V$ is the characteristic time of propagation of a crack of length L at the velocity V. Since in our experiments R_{tip} is

comparable with L and the fracture propagation time t^* is much shorter than the relaxation time τ, the energy dissipation originating from this term can be considered as negligible in front of the surface energy term $J = 2\gamma_s$.

The $r^{-1/2}$ component $\sigma_{12}^{(C)}$ gives the contribution $G_V^{(12)}(V)$ to the viscous dissipated energy:

$$G_V^{(12)}(V) \sim \frac{V}{2\mu_\infty \tau}\int_{\omega_{min}}^{\omega_{max}} \left(\sigma_{12}^{(C)}\right)^2 \frac{d\omega}{\omega^3} \simeq J\frac{t^*}{\tau} \qquad (12)$$

We recover the prediction of the trumpet model for the linear case where $J = G_0$.

The r^{-1} component $\sigma_{22}^{(C)}$ gives the contribution $G_V^{(22)}(V)$ to the viscous dissipated energy:

$$G_V^{(22)}(V) \sim \frac{V}{2\mu_\infty \tau}\int_{\omega_{min}}^{\omega_{max}} \left(\sigma_{22}^{(C)}\right)^2 \frac{d\omega}{\omega^3} \simeq \frac{\mu_\infty a^4}{\tau}\ln\frac{L}{l} \qquad (13)$$

By using (31) again, we can derive the scaling law from (13):

$$\frac{G_V^{(22)}(V)}{J} \sim \frac{J}{\mu_\infty V\tau}\ln\frac{L}{l} \sim \frac{R_{tip}}{V\tau}\ln\frac{L}{l} \sim \frac{R_{tip}}{L}\frac{t^*}{\tau}\ln\frac{L}{l} \qquad (14)$$

Once again this dissipated energy is negligible in our experiments since R_{tip} is comparable with L and the fracture propagation time t^* is much shorter than the relaxation time τ. Note however the low logarithmic dependence of $G_V^{22}(V)$ with L.

We remark that the necessary conditions for neglecting bulk viscous dissipations in the fracture energy of a Maxwell fluid are more restrictive in the hyperelastic regime than in the simple elastic linear case. Eqns (11), (12) and (13) show that the main condition for neglecting bulk viscous dissipation is that the characteristic time t^* of the opening of crack of length L should much smaller that the relaxation time of the Maxwell fluid τ, as it is in the simple elastic linear regime. However, a new length scale $R_{tip} \sim J/\mu_\infty \sim a^2$ – the radius of curvature of the crack tip, or equivalently the size of the large strain region – becomes relevant. The dissipated energy can sensibly be neglected only when the length of the crack is of the same order of magnitude than R_{tip} as in our experiments. For very short cracks ($L < R_{tip}$) eqn (14) predicts the term $G_V^{(22)}$ to become important, while for longer cracks ($R_{tip} < L < V\tau$) eqn (11) predicts the term $G_V^{(11)}$ to become important.

5 Microscopic model for the fracture velocity

In the following we will only focus on the first regime, where both the fracture energy G and the crack velocity V are constant in time ($L \lesssim 0.1D_0$) and also take approximately the same value $V \sim$ mm s^{-1} in the two fluids R6 and R12 (Fig. 6). We remark that $V \ll c_R$, $c_R \approx \sqrt{\mu_\infty/\rho}$ (of the order of 1 m s^{-1}) being the speed of sound in the medium. What is the mechanism that explains this low speed propagation?

Basically, we argue that the scaling of the velocity V of the fracture is given by the characteristic speed of relaxation of a microemulsion droplet at the opening crack interface, under the action of the unbalanced elastic force of the polymer bridge towards the gel (Fig. 8). This velocity is given by balancing the elastic force and the viscous drag force acting on the droplet (Reynolds number $R_e \ll 1$).

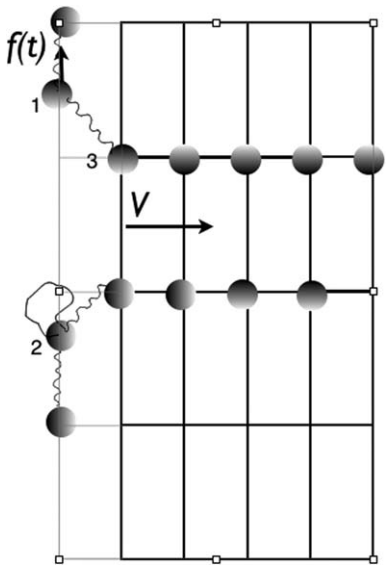

Fig. 8 A cartoon of the viscous relaxation mechanism of a bead at the tip of the fracture. The polymer bridge between beads (1) and (2) just debonded, forming a loop on bead (2). Bead (1) thus experiences the spring-back force $f(t)$ due to the gel under tension; this will lead to an increasing extra tension on bead (3) and crack propagation at velocity V.

Just before the bead at the tip of the fracture is released (at time $t = 0$) by the debonding of a polymer bridge, it is submitted to the normal force:

$$f_0 = \frac{\sigma_i d_0^2}{\lambda_i} \qquad (15)$$

where $\lambda_i = d_i/d_0$ is the elongation of the network at the crack tip, d_0 is the mean distance between droplets at rest ($d_0 \simeq (4\pi\phi/3)^{1/3}b$), η_W is the viscosity of the water and σ_i is the local normal stress at the tip of the fracture. Note that eqn (15) assumes the incompressibility of the gel. For $t > 0$, the bead experiences the following springback force due to the gel under tension (Fig.8):

$$f(t) = \frac{\sigma(t) d_0^2}{\lambda(t)} \qquad (16)$$

From the relationship between $\sigma(t)$ and $\lambda(t) = d(t)/d_0$ given by the affine network model of the unentangled rubber elasticity theory,[32] one gets:

$$f(t) = \frac{Ed_0^2}{3}\left(\lambda(t) - \frac{1}{\lambda^2(t)}\right) \qquad (17)$$

The size of the bead is submicrometric, and so its motion in water obeys the Stokes law:

$$6\pi\eta_W b d_0 \frac{d\lambda}{dt} = f(t) \qquad (18)$$

where η_W is the viscosity of water. Substituting (17) in (18) and integrating the obtained differential equation with the initial condition given by (15) gives:

$$\lambda(t) = [1 + (\lambda_i^3 - 1)\exp(-t/\tau_1)]^{1/3} \qquad (19)$$

with a characteristic time

$$\tau_1 = \frac{6\pi\eta_W R}{Ed_0} \quad (20)$$

To obtain the characteristic fracture velocity, one can estimate that the next bead will debond (causing the growth of the fracture of length d_0/λ_i) when $\lambda = f_d\lambda_i$, where $\lambda_i^{-1} \leq f_d \leq 1$ is a critical elongation felt by the chain on the next bonded bead, that is difficult to estimate. Indeed, the relaxation of the debonded bead induces extra elastic tensions on the next bead at the tip of the fracture that will grow with time. The time necessary to reach this critical elongation is then according to eqn (19):

$$t_p = \tau_1 \ln\left[\frac{\lambda_i^3}{f_d\lambda_i^3 - 1}\right] \quad (21)$$

The time scale is thus given by eqn (21) with logarithmic corrections. Finally the fracture velocity is:

$$V = \frac{d_0}{\sqrt{\lambda_i}}\frac{1}{t_p} = \frac{Ed_0^2}{6\pi\eta_w b}\left[\sqrt{\lambda_i}\ln\left(\frac{\lambda_i^3 - 1}{f_d\lambda_i^3 - 1}\right)\right]^{-1} \quad (22)$$

The function g: $\lambda_i \rightarrow \left[\sqrt{\lambda_i}\ln\left(\frac{\lambda_i^3 - 1}{f_d^3\lambda_i^3 - 1}\right)\right]^{-1}$ exhibits a maximum whose position and value depend on f_d and determines an upper bound for the fracture velocity. We choose $f_d = 0.5$. Indeed $2 < \lambda_i < 8$ ($\lambda_i = 2$corresponds roughly to the maximal macroscopic elongation for the network experimentally observed before rupture occurs in pendant drop experiments and $\lambda_i \cong 8$[33] corresponds to the maximal elongation usually observed in permanent rubbers), one gets $\max(g) = \alpha = 0.25$. We note that $\max(g)$ is a decreasing function of f_d. So the choice $f_d = 0.5$ will give the upper limit for the estimation of the crack velocity:

$$V \lesssim 0.25\frac{Ed_0^2}{6\pi\eta_W b} \quad (23)$$

6 Discussion of the experimental results

For the fluids R6 and R12, the relaxation time τ is, respectively, 0.6 and 2 s. The upper bound value of the crack length is the initial diameter $D_0 = 0.6$ mm of the filament when the rupture process begins, that is $L(t) < 0.6$ mm. The crack velocity was found to be constant at $V \simeq 4$ mm s^{-1}. For both fluids, the characteristic time of a fracture event $t^* < 0.15$ s. The condition $(t^*/\tau) < 1$ is thus fulfilled (note that in fact, as discussed in section 3, the experimental analysis we did is valid for $L < 0.1D_0$ so that $t^*/\tau < 0.025$). The radius of curvature of the crack tip is given, respectively, by $R_{tip} = a^2/2 \simeq 174$ and 24 μm, which are of the same order of magnitude as the observed crack lengths.

Therefore the response of the material is completely elastic ($L < V\tau$), the size of the sample being too small or, equivalently, the time necessary to fracture the filament is to small ($t^* < \tau$) to see any viscous dissipation on the overall rupture phenomenon. The fracture energy is thus expected to be independent of crack speed and to equal $G_0 = 2\gamma = 2(\gamma_s + \gamma_{pol})$. The first term is the classical Dupré work needed to form two new air/gel surfaces (dry fracture). However, before dry fracture occurs by instability of the capillary bridge, the wet fracture must have already occurred and its interfacial cost is $2\gamma_{pol}$. As reported in a previous work,[12] this term of purely entropic origin is related to the loss of conformational entropy of polymer chains at the crack surface $\gamma_{pol} \simeq (\ln 2/2)k_BTN_P^{2/3}$, where $N_P \approx 3\phi r/8\pi b^3$ is the number density of polymer chains in the sample (*cf.* Fig. 1). This interfacial tension is extremely low and roughly equal to 10 μN m^{-1} and is thus negligible compared to the air/gel interfacial tension $\gamma_s \simeq 45$ mN m^{-1}. It has been proved that for many systems G_0 exhibits a marked dependence on V, and most of the rate dependence of $G(V)$ then originates from the rate dependence of G_0 itself.[34] Raphael and de Gennes[35] have shown theoretically that the surface energy required to debond the connectors between two surfaces is indeed velocity dependent. However, in our fluid this argument would apply to the component γ_{pol} which is negligible in front of the dominant term γ_s, thus resulting in a substantial independence of G_0 from V.

Although the condition $L < V\tau$ is respected throughout the experiment, the trumpet model can only accurately describe the first observed regime of crack propagation where $L < 0.1D_0$. This is not surprising, since the modeling is relative to the fracture propagation in a semi-infinite medium. The second regime for $L > 0.1D_0$ must clearly be attributed to the finite size of the soft filament and to the increasing value of the strain in the progressively thinning ligament (*cf.* Fig. 5) leading to the progressive failure of the rough 2D approximation. The increase of G for long cracks could partially be caused by the hyperelastic dissipation term $G_V^{(11)}$ predicted by eqn (11), but a more accurate mechanical modelling would be needed to explore this possibility.

For both R6 and R12 fluids, the value of the crack velocity fluid ($V = 4$mm s^{-1}, Fig. 6) is in good agreement with inequality (23) that gives $V \sim 6$ mm s^{-1} for a reasonable expected value $\alpha \sim 0.25$. This strongly supports our hypothesis that the kinetics of the crack propagation are governed by the elastic relaxation of the oil droplets after a debonding event, under the action of the viscous drag of the solvent. Note that the control of the crack velocity by network/solvent friction has been already proposed by Baumberger *et al.*[4,36] in the viscoplastic fracture dynamics of an other class of reversible gels, *i.e.* gelatin.

7 Conclusions

We performed an original experimental investigation of the brittle fracture of a viscoelastic Maxwell fluid using a pendant drop experiment. This configuration allows for an excellent reproducibility of the fracture initiation and propagation, as well as a pure elongational stress condition due to the lack of contact with solid interfaces near the fracture region. The fracture of the fluid happens in two steps. The fracture initiation step, discussed in a previous work,[12] was shown to be governed by the thermally activated nucleation of a critical crack in the polymer network. The second step, consisting in the rapid propagation of a brittle fracture in the fluid, was analysed in detail here and shown to be energetically governed by the surface tension of the solvent (oil-in-water droplet microemulsion).

According to the viscoelastic trumpet model of de Gennes, the absence of bulk viscous dissipation was justified by the short length of the crack in relation to the characteristic length $V\tau$ where the viscous dissipation starts to become effective. Moreover, an extension of the trumpet model to hyperlasticity has allowed us to confirm the weakness of the dissipated energy in terms of a new relevant length scale $R_{tip} \sim G_0/\mu_\infty$, which is found

to be of the same order of magnitude as the observed crack lengths. In agreement with this interpretation, the measured crack opening profiles presented a constant parabolic shape, which can be related by nonlinear fracture mechanics to a fracture energy equalling the Dupré energy for the creation of the two solvent surfaces $G_0 = J = 2(\gamma_s + \gamma_{pol}) \approx 2\gamma_s$. The fact that the contribution of the polymer network to the surface tension of the fluid is negligible, was shown to be the cause of the extreme brittleness of the fracture propagation. In fact, the different sources of local dissipation in the small nonlinear zone were shown to be of the same order as γ_{pol} and are thus energetically negligible during crack propagation.

On the other hand, the slow velocity of crack propagation ($V \approx 4\ \mathrm{mm\ s^{-1}} \ll c_R$) was shown to be governed by the time scales of the local crack tip debonding processes, and namely by the elastic relaxation time of the oil droplets after a debonding event under the action of the viscous drag of the solvent. The remarkable properties of this original model system were thus shown to be related to the excellent degree of uncoupling between the energetic and kinetic properties of the fracture propagation, due to the presence of a dominant solvent energy term in the surface tension of the fluid.

Appendix 1: Large strain crack tip solutions in plane strain condition

Let $\mathbf{x}$ and $\mathbf{y}$ be the coordinates of the physical points in the non deformed and deformed frames according to:

$$\mathbf{y} = \hat{\mathbf{y}}(\mathbf{x}) = \mathbf{x} + \mathbf{u}(\mathbf{x})$$

where $\mathbf{u}(\mathbf{x})$ is the displacement field (expressed in the non deformed frame). The first order terms of the 2D plane strain non-linear elastic solution for the crack tip fields in a Neo-Hookean soft solid were provided by Stephenson:[21]

$$y_1 = -\frac{b_2}{a} r \sin^2\frac{\theta}{2} \tag{24}$$

$$y_2 = a\sqrt{r}\,\sin\frac{\theta}{2} \tag{25}$$

where $\mathbf{y}=(y_1,y_2)$ and $\mathbf{x}=(r,\theta)$, while a and b_2 are two dimensioned constants. The J integral is computed in the non deformed frame according to:

$$J = \int_{\Gamma\varepsilon}[Wn_1 - \sigma_{\alpha\beta}n_\beta u_{\alpha,1}]\mathrm{d}s \tag{26}$$

where $\vec{n} = (n_1, n_2) = (\cos\theta, \sin\theta)$ is the normal vector to the surface Γ_ε (which is a circle of radius ε around the crack tip, $\mathrm{d}s = \varepsilon \mathrm{d}\theta$ is the length increment, σ is the nominal Piola stress and the elastic energy density function is:

$$W(I) = \frac{\mu}{2}(I - 3) \tag{27}$$

$I = tr(G)$is the invariant of the left Cauchy–Green strain tensor $G_{ik} = FF^T$, where $F_{ij} = y_{i,j}$ is the deformation gradient.

According to Stephenson,[21] the nominal Piola stress (expressed in the non deformed frame) can be derived from:

$$\sigma^{(P)} = 2W'(I)F - pF^{-T} \tag{28}$$

where p is the crack tip pressure field:

$$p = -\frac{2\mu b}{a^2}\cos\frac{\theta}{2} + \frac{2\mu}{a^2} r(3 - \cos\theta) + o(r) \tag{29}$$

For the computation of the J integral, we only need to retain singular terms. Since the pressure field is bounded, the nominal stress reduces to:

$$\sigma^{(P)} = \mu F = \mu \begin{bmatrix} -\frac{b_2}{a}\sin^2\frac{\theta}{2} & -\frac{b_2}{a}\sin\frac{\theta}{2}\cos\frac{\theta}{2} \\ -\frac{a}{2\sqrt{r}}\sin\frac{\theta}{2} & \frac{a}{2\sqrt{r}}\cos\frac{\theta}{2} \end{bmatrix} \tag{30}$$

$$J = \int_{\Gamma_\epsilon} \sigma_{\alpha\beta} n_\beta u_{\alpha,1}\mathrm{d}s = \frac{\mu a^2}{4}\int_0^{2\pi}\frac{1}{\epsilon}\epsilon\sin^2\frac{\theta}{2}\mathrm{d}\theta = \frac{\pi\mu a^2}{4} \tag{31}$$

The equations for the deformed crack profile (24 and 25) can be combined to express the visual parabolic contour line of the deformed crack lips:

$$y_2 = a\sqrt{\frac{-y_1}{C}} \tag{32}$$

where we defined the dimensionless coefficient $C = b_2/a$. Since C is found to be close to 1 in the FE simulations especially in large strain,[20] we can directly relate the opening parameter of the parabola to J by inverting (31):

$$a = \sqrt{\frac{4J}{\pi\mu}} \tag{33}$$

If we express the solutions for the true Cauchy stress tensor in the non deformed frame:[21]

$$\sigma^{(C)} = \mu \begin{bmatrix} C^2 & -\frac{a}{2\sqrt{r}}\sin\frac{\theta}{2} \\ -\frac{a}{2\sqrt{r}}\sin\frac{\theta}{2} & \frac{a^2}{4r} \end{bmatrix} \tag{34}$$

we remark the different scaling of the components of the Cauchy and Piola stress tensors. In particular the $\sigma_{11}^{(C)}$ term is bounded, while the $\sigma_{22}^{(C)}$ presents a $1/r$ singularity. For the sake of estimating physical scaling laws for the energy dissipation, the true Cauchy stress is certainly the most relevant quantity.

Appendix 2: Viscous dissipation in the nonlinear zone of the fracture

The debonding of a polymer bridge under tension leads to a viscous dissipation due both to the motion of bead 3 in Fig. 8 in the solvent and to the friction of the polymer bridge linking beads 1 and 3 with the solvent too. Both forms of dissipated energy will be of the same order of magnitude, the polymer contribution being even smaller since the hydrodynamic radius of the polymer chain is $R_H \sim 4\ \mathrm{nm} < b$.

We focus here to the viscous dissipation due to the motion of a bead 3 in font of the fracture tip that will dissipate energy. The corresponding energy cost has been already calculated in section 5:

$$E_d \simeq \int_{\lambda i}^{1} f(t) d_0 d\lambda \tag{35}$$

where $f(t)$ is given by eqn (17). This leads to a dissipative contribution to the fracture energy ΔG_0:

$$\Delta G_0(V) \approx (N_p/2)^{2/3} \frac{Ed_0^3}{2} = \frac{1}{3}(\pi/12)^{1/3} \frac{r^{2/3} bE}{\phi^{1/3}} \qquad (36)$$

where we have assumed that roughly half of the polymer chains are in bridge configuration[37] and that $\lambda_i = 2$. For the fluid R12 ($\phi = 10\%$, $R = 12$), $\Delta G_0(V) \sim 35$ μJ m^{-2} $\ll 2\gamma_s$, which is once again of the same order as γ_{pol} and is thus negligible in front of the dominant term $2\gamma_s$.

Acknowledgements

We thank G. Porte and C. Fretigny for stimulating discussions. This work has been supported by the ANR (contract No. ANR-06-BLAN-0097(TSANET)).

References

1 A. A. Griffith, *Phil. Trans. Roy. Soc. London*, 1921, **A221**, 163–198.
2 A. N. Gent and J. Shultz, *J. Adhes.*, 1972, **3**, 281.
3 E. H. Andrews and A. Kinloch, *J. Proc. R. Soc. (London)*, 1973, **401**, A332–385.
4 T. Baumberger, C. Caroli and D. Martina, *Nat. Mater.*, 2006, **5**, 552.
5 M. E. Seitz, D. Martina, T. Baumberger, V. R. Krishnan, C. Hui and K. Shull, *Soft Matter*, 2009, **5**, 447.
6 P. Cordier, F. Tournhilac, C. Soulié-Zakovich and L. Leibler, *Nature*, 2008, **451**, 0669.
7 C. L. Mowery, A. J. Crosby, D. Ahn and K. R. Shull, *Langmuir*, 1997, **13**, 6101.
8 A. Tripathi, K. C. Tam and G. H. McInley, *Macromolecules*, 2006, **39**, 1981.
9 A. Bhardwaj, E. Miller and J. P. Rothstein, *Rheol. Acta*, 2007, **51**, 693.
10 A. Bhardwaj, D. Richter, M. Chellamuthu and J. P. Rothstein, *J. Rheology*, 2007, **46**, 86.
11 H. Tabuteau, S. Mora, L. Ramos, G. Porte and C. Ligoure, *Prog. Theor. Phys., Suppl.*, 2008, **175**, 47.
12 H. Tabuteau, S. Mora, G. Porte, M. Abkarian and C. Ligoure, *Phys. Rev. Lett.*, 2009, **102**, 155501.
13 S. Mora, *Soft Matter*, 2011, **7**, 4908.
14 T. Tixier, H. Tabuteau, A. Carrière, L. Ramos and C. Ligoure, *Soft Matter*, 2010, **6**, 2699.
15 J.-F. Berret and Y. Serero, *Phys. Rev. Lett.*, 2001, **87**, 048303.
16 P. Skrzeszewska, J. Sprakel, F. de Wolf, R. Fokkink, M. A. Cohen Stuart and J. van der Gucht, *Macromolecules*, 2010, **43**, 3542.
17 F. Saulnier, T. Ondarçuhu, A. Aradian and R.E., *Macromolecules*, 2004, **37**, 1067–1075.
18 E. Michel, M. Filali, R. Aznar, G. Porte and J. Appell, *Langmuir*, 2000, **16**, 8702.
19 J. Sprakel, N. A. M. Besseling, F. A. M. Leermakers and M. A. Cohen Stuart, *Phys. Rev. Lett.*, 2007, **99**, 104504.
20 V. R. Krishnan, C. Y. Hui and R. Long, *Langmuir*, 2008, **24**, 14245.
21 R. A. Stephenson, *J. Elasticity*, 1992, **12**, 65–99.
22 L. B. Freund, *Dynamic Fracture Mechanics*, Cambridge University Press, Cambridge, 1990.
23 M. Filali, R. Aznard, M. Svensson, G. Porte and J. Appell, *J. Phys. Chem. B*, 1999, **103**, 7293.
24 Y. M. Stokes, E. O. Tuck and L. W. Schwartz, *Q. J. Mech. Appl. Math.*, 2000, **53**, 565.
25 L. B. Smolka, A. Belmonte, D. Henderson and T. P. Witelski, *Eur. J. Appl. Math.*, 2004, **15**, 679.
26 G. R. Irwin, *J. Appl. Mech.*, 1957, **24**, 361–364.
27 C. Y. Hui, A. Jagota, S. J. Bennison and J. D. Londono, *Proc. R. Soc. London, Ser. A*, 2003, **459**, 1489–1516.
28 J. Rice, *J. Appl. Mech.*, 1968, **35**, 379–386.
29 P.-G. de Gennes, *CR Acad. Sci. Paris Srie II*, 1988, **307**, 1949.
30 P.-G. de Gennes, *Langmuir*, 1996, **12**, 4497–4500.
31 M. L. Williams, R. F. Landel and J. D. Ferry, *J. Am. Chem. Soc.*, 1995, **77**, 3701.
32 M. Rubinstein and R. H. Colby, *Polymer Physics*, Oxford University Press, New York, 2003.
33 L. R. G. Treloar, *The physics of rubber elasticity*, 3rd edition, Clarendon Press, Oxford, 1975.
34 A. N. Gent, *Langmuir*, 1996, **12**, 4492.
35 E. Raphaël and P. de Gennes, *J. Phys. Chem.*, 1992, **96**, 4002.
36 T. Baumberger, C. Caroli and D. Martina, *Eur. Phys. J. E*, 2006, **21**, 81.
37 V. Testard, J. Oberdisse and C. Ligoure, *Macromolecules*, 2008, **41**, 7219.

